A Self-Locomotive Soft Actuator Based on Asymmetric Microstructural $Ti_3C_2T_x$ MXene Film Driven by Natural Sunlight Fluctuation

Ying Hu,[1,2] Lulu Yang,[1] Qiuyang Yan,[3,4] Qixiao Ji,[1] Longfei Chang,[1] Chenchu Zhang,[1] Jian Yan,[2] Ranran Wang,[3*] Lei Zhang,[5] Guan Wu,[6*] Jing Sun,[3] Bin Zi,[1] Wei Chen,[7] and Yucheng Wu[4]*

1. Anhui Province Key Lab of Aerospace Structural Parts Forming Technology and Equipment, Institute of Industry & Equipment Technology, Hefei University of Technology, Hefei, 230009, P. R. China

2. Key Laboratory of Advanced Functional Materials and Devices of Anhui Province, School of Materials Science and Engineering, Hefei University of Technology, Hefei, 230009, P. R. China

3. State Key Laboratory of High Performance Ceramics and Superfine Microstructure, Shanghai Institute of Ceramics, Chinese Academy of Science, Shanghai, 200050, P. R. China

4. University of Chinese Academy of Sciences, Beijing, 100049, P. R. China

5. Anhui Key Laboratory of Condensed Matter Physics at Extreme Conditions, High Magnetic Field Laboratory, Chinese Academy of Sciences, Hefei, 230031, P. R. China

6. State Key Laboratory of Materials-Oriented Chemical Engineering, College of Chemical Engineering, Nanjing Tech University, Nanjing, 211816, P. R. China

7. Research Centre for Smart Wearable Technology, Institute of Textiles and Clothing, The Hong Kong Polytechnic University, Hong Kong, 999077, P. R. China

---

* Author to whom any correspondence should be addressed E-mail: huying@hfut.edu.cn, wangranran@mail.sic.ac.cn, gwu2016@njtech.edu.cn.

Supporting Information

Figure S1. The Tyndall scattering effect of the MXene solution.

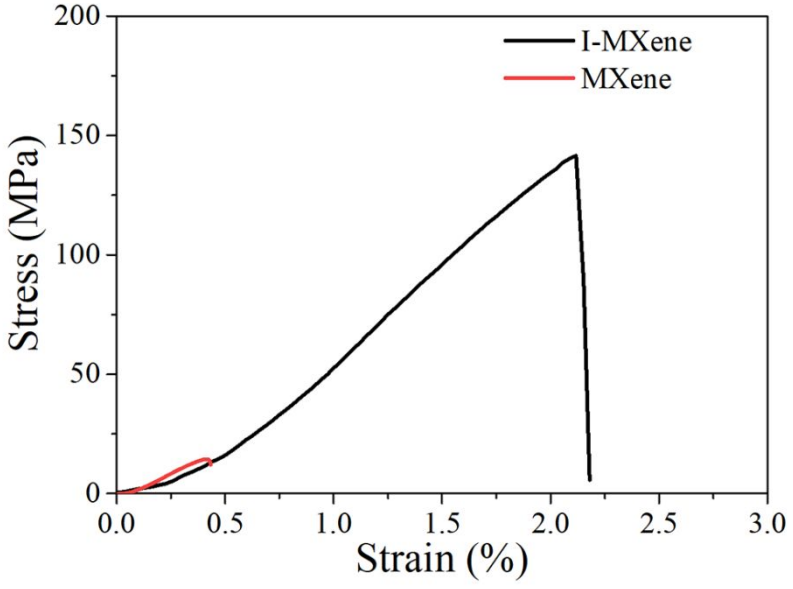

Figure S2. The stress-strain curves of the I-MXene film and pure Mxene film.

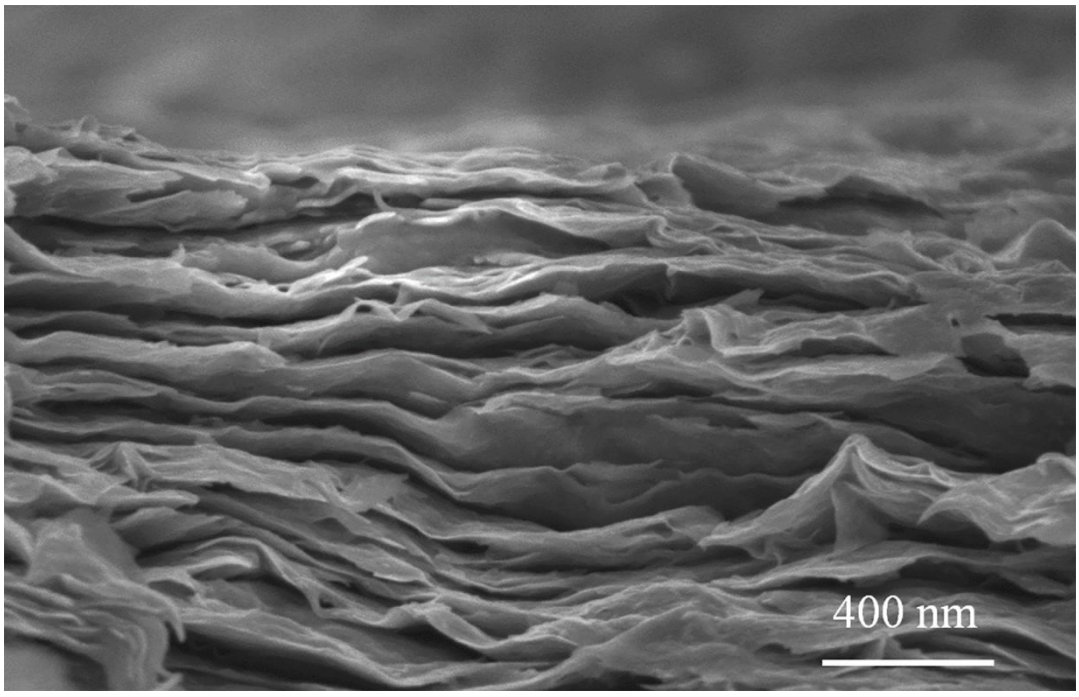

Figure S3. A magnified cross-sectional SEM image of the I-Mxene film.

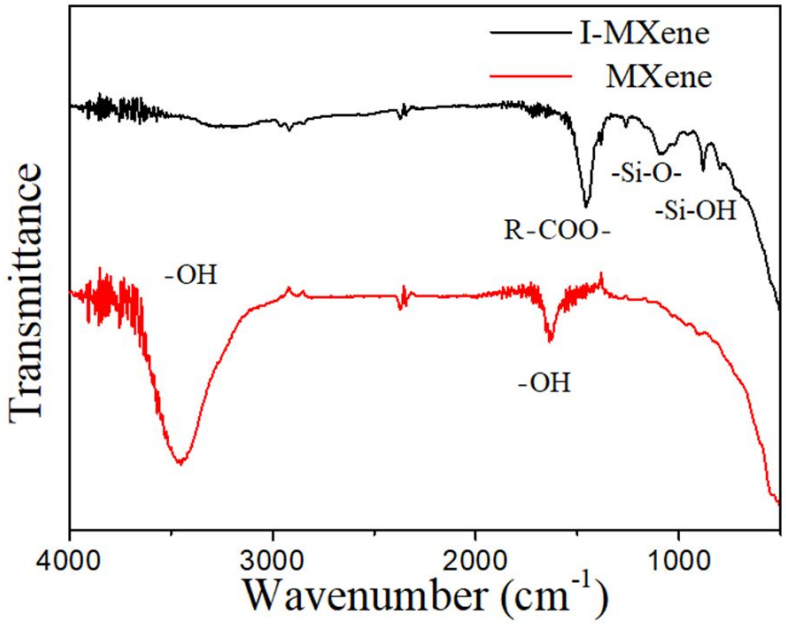

Figure S4. FTIR spectra of the I-MXene and pure Mxene.

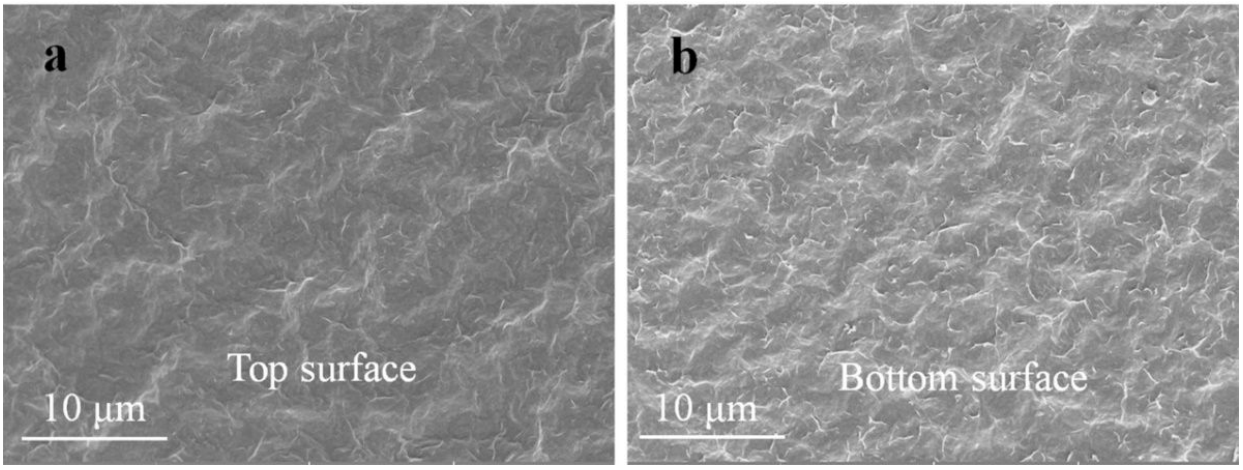

Figure S5. SEM images of the (a) top and (b) bottom surfaces of the I-MXene film.

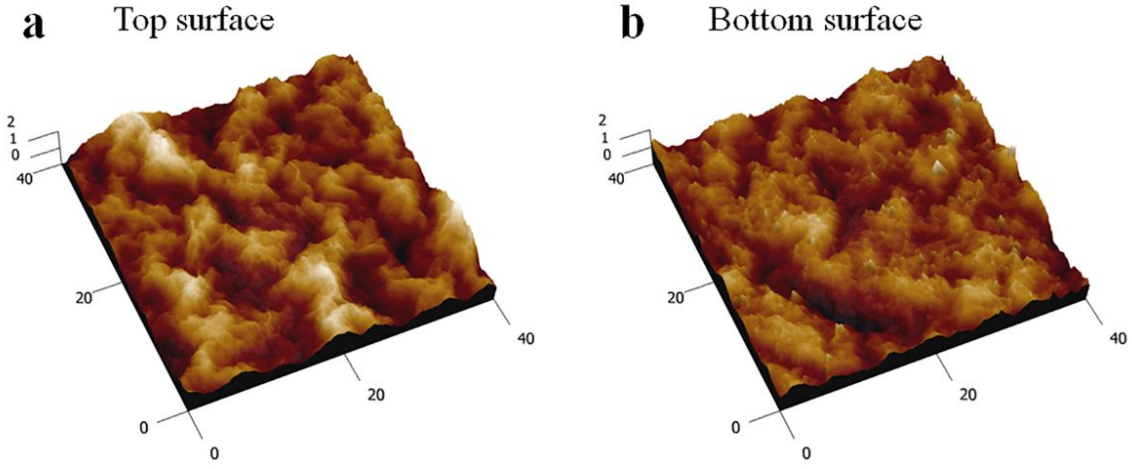

Figure S6. AFM images of the (a) top and (b) bottom surface morphologies of the I-MXene film.

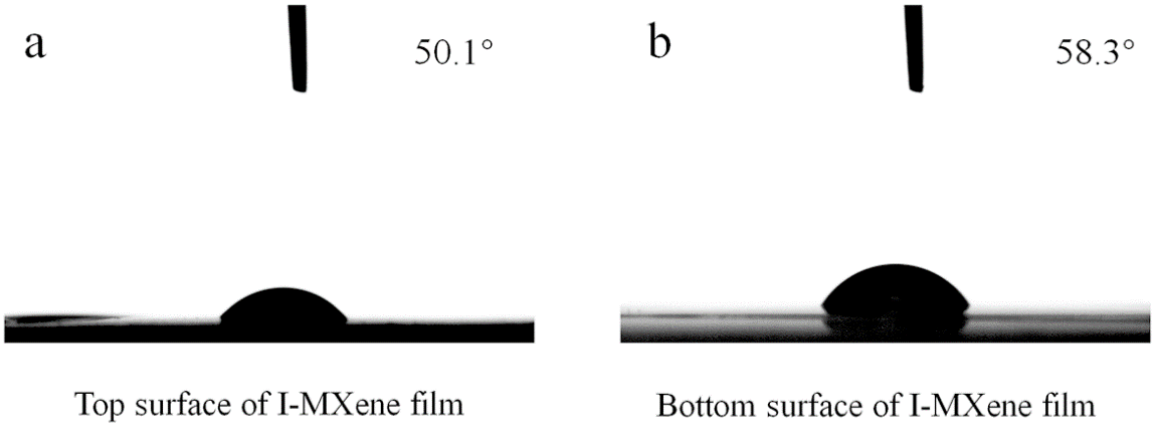

Figure S7. Comparison for the water contact angles of the (a) top surface of the I-MXene film with that of the (b) bottom surface of the I-MXene film.

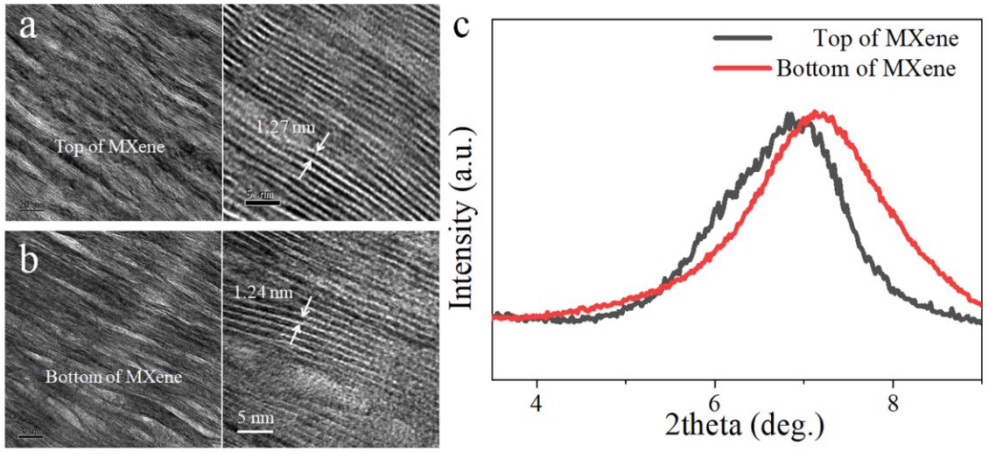

Figure S8. (a, b) HRTEM images of the top and bottom regions of the unmodified pure MXene film, respectively. (c) XRD patterns of the top and bottom of the pure MXene film.

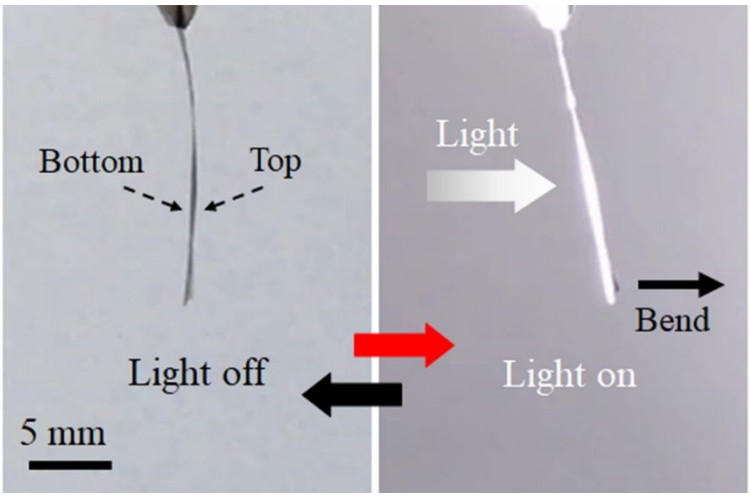

Figure S9. Light-driven reversible deformation of the freestanding I-MXene film. The light is incident from the left side.

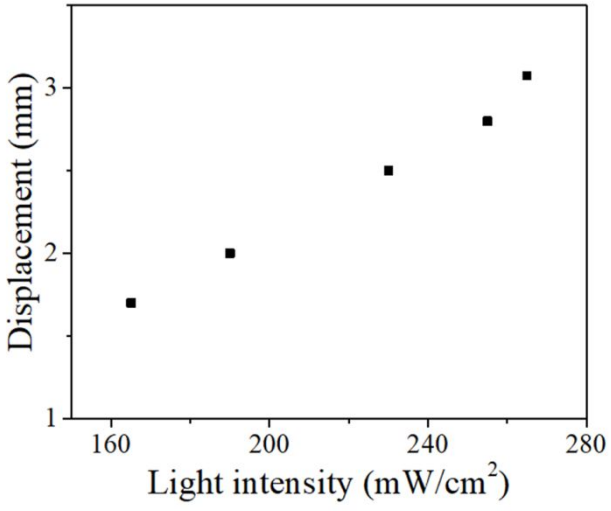

Figure S10. Maximal bending displacement of the I-MXene film under light irradiation with different light intensity.

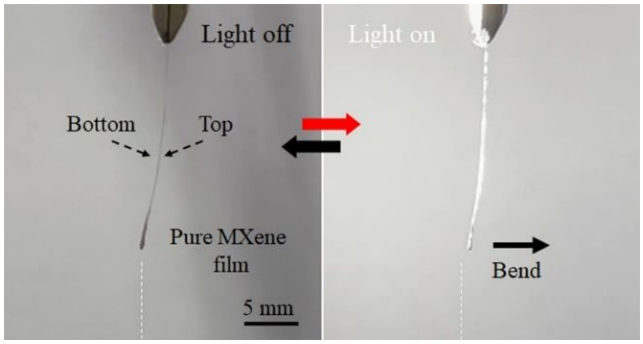

Figure S11. Light-driven reversible deformation of the freestanding pure MXene film at the same stimulation conditions with that of the I-MXene film. Here the light intensity is about 265 mW/cm^2, the maximal temperature is about 70 ℃, and the relative humidity is about 55%.

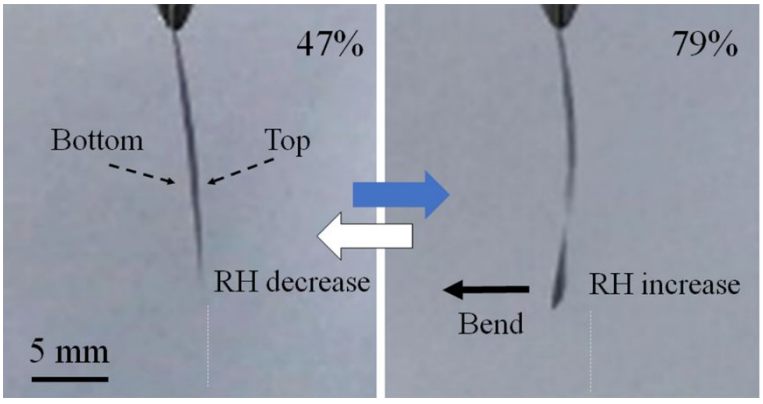

Figure S12. Deformation of the freestanding I-MXene film in response to the RH change.

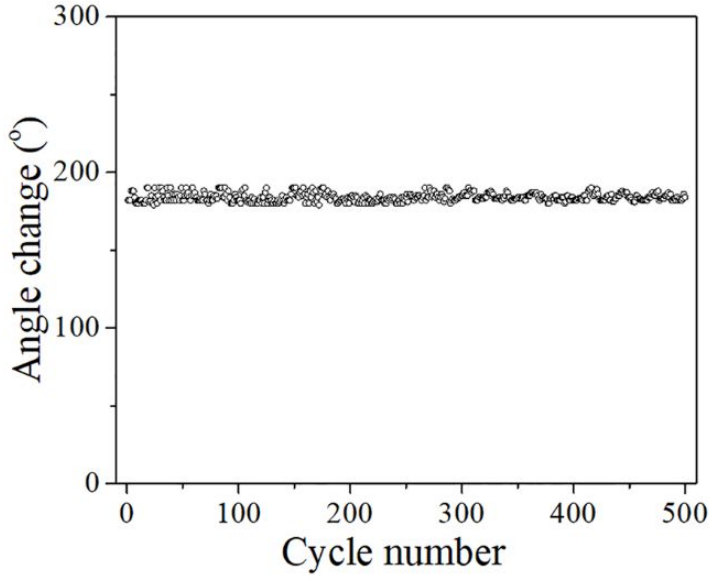

Figure S13. Cyclic actuation of the bimorph actuator under the simulated sunlight irradiation (45 mW/cm^2).

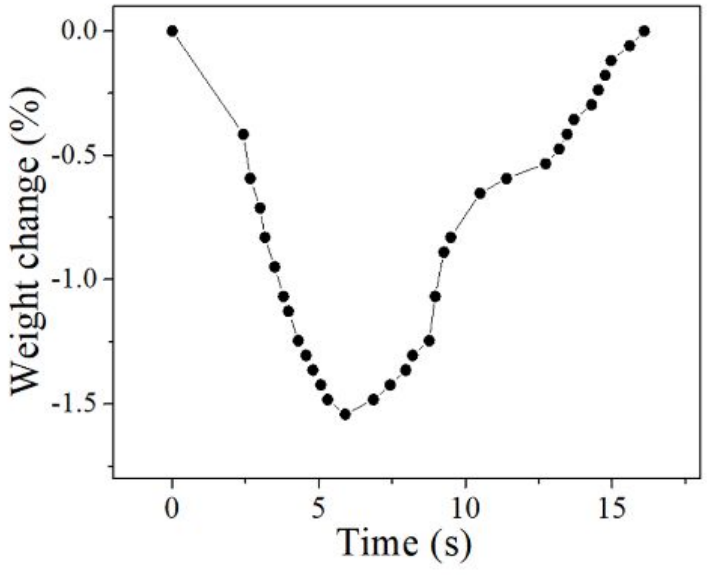

Figure S14. Real-time weight change of the bimorph actuator during the light-driven actuation process.

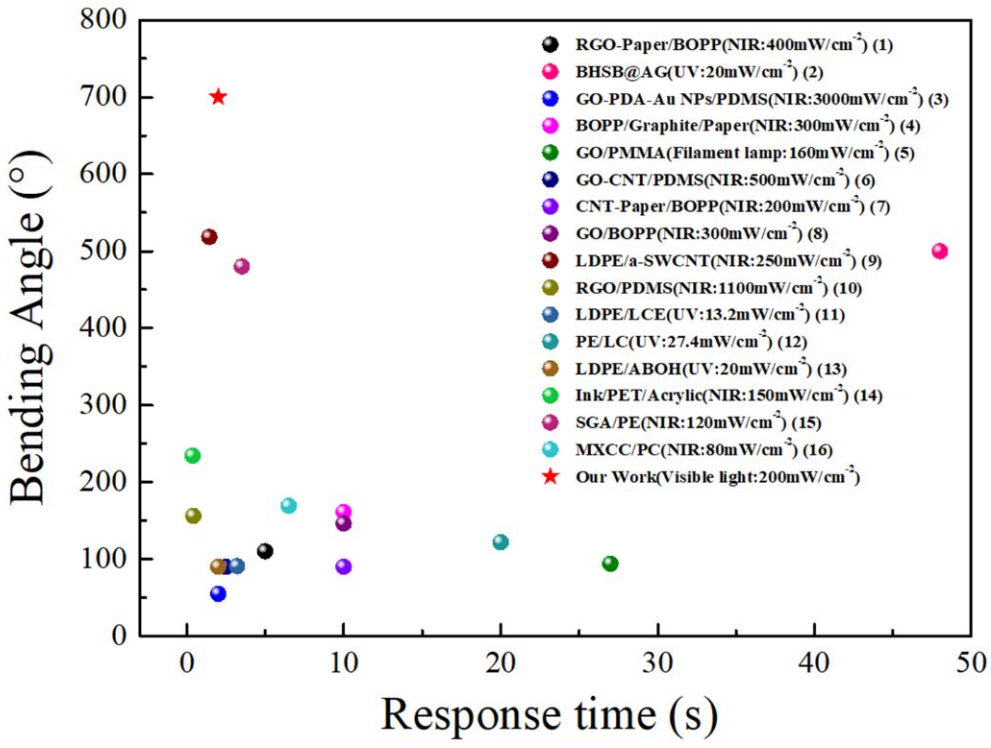

Figure S15. Comparison of recent reported photoactuators and our I-MXene/PE bimorph actuators on light-driven bending angle *vs*. response time.

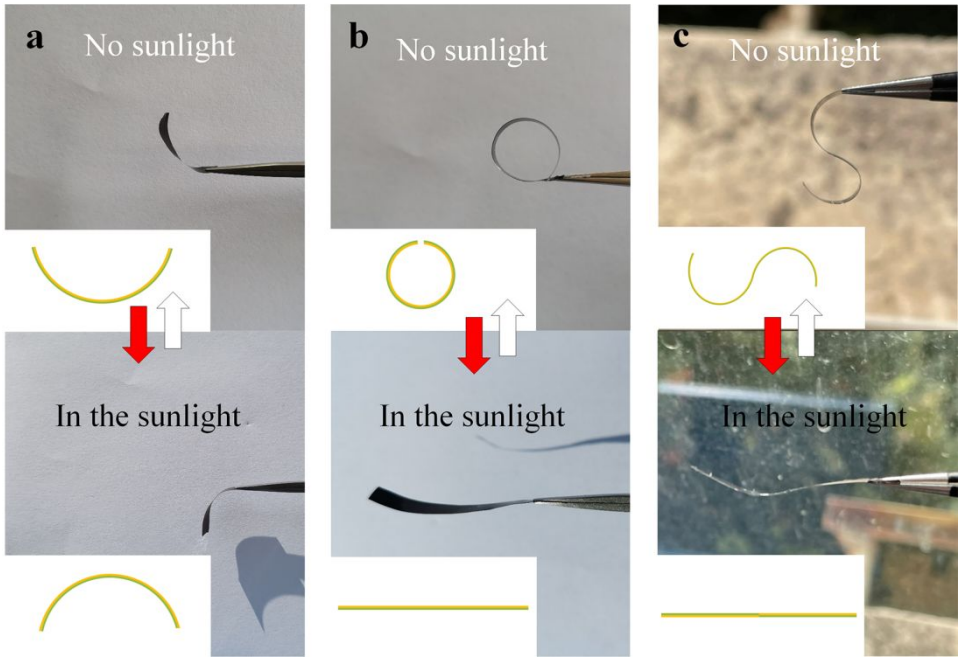

Figure S16. Natural sunlight-driven actuation of the bimorph actuators with different original shapes by the heat setting method. (a) Reversible upward bending-to-downward bending deformation with natural sunlight off and on. (b) Reversible circular-to-straight deformation with natural sunlight off and on. (c) Reversible S-shape-to-straight deformation with natural sunlight off and on.

Figure S17. Optical image of the biomimetic “inchworm” robot disguise as an inchworm on a fallen leaf in the wild environment.

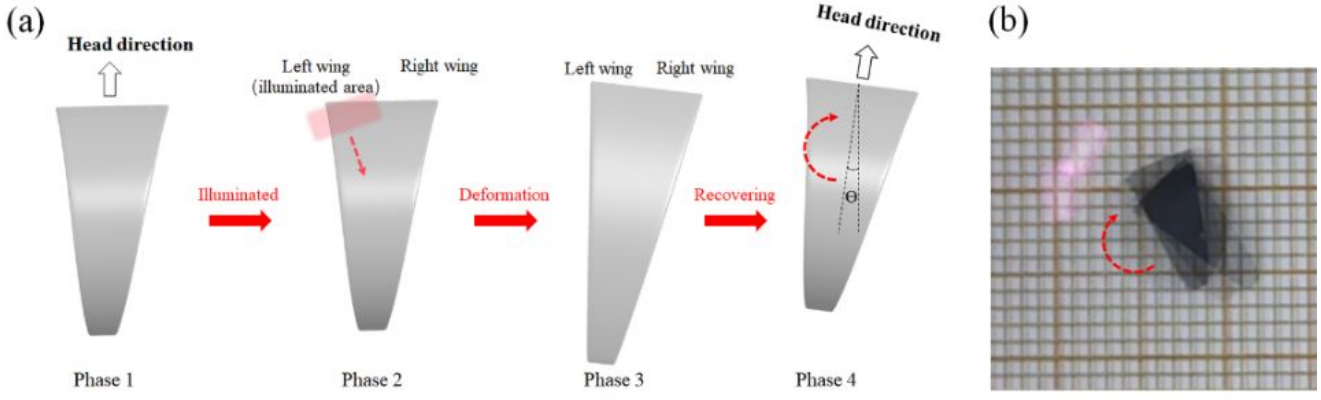

Figure S18. (a) Schematic diagram of the rotation motion controlled by the laser. (b) Superimposed images of the turning motion of the soft robot under the laser scanning.

REFERENCES

(1) Chen, L.; Weng, M.; Zhou, P.; Huang, F.; Liu, C.; Fan, S.; Zhang, W. Graphene-Based Actuator with Integrated-Sensing Function. *Adv. Funct. Mater.* **2019**, 29, 1806057-1806065.

(2) Zhang, L.; Naumov, P. Light- and Humidity-Induced Motion of an Acidochromic Film. *Angew. Chem. Int. Ed.* **2015**, 54, 8642-8647.

(3) Yang, Y.; Liu, Y.; Shen, Y. Plasmonic-Assisted Graphene Oxide Films with Enhanced Photothermal Actuation for Soft Robots. *Adv. Funct. Mater.* **2020**, 30, 1910172-1910178.

(4) Weng, M.; Zhou, P.; Chen, L.; Zhang, L.; Zhang, W.; Huang, Z.; Liu, C.; Fan, S. Multiresponsive Bidirectional Bending Actuators Fabricated by a Pencil-on-Paper Method. *Adv. Funct. Mater.* **2016**, 26, 7244-7253.

(5) Gao, Y.; Zhang, Y.; Han, B.; Zhu, L.; Dong, B.; Sun, H. Gradient Assembly of Polymer Nanospheres and Graphene Oxide Sheets for Dual-Responsive Soft Actuators. *ACS Appl. Mater. Interfaces* **2019**, 11, 37130-37138.

(6) Wang, W.; Xiang, C.; Zhu, Q.; Zhong, W.; Li, M.; Yan, K.; Wang, D. Multistimulus Responsive Actuator with GO and Carbon Nanotube/PDMS Bilayer Structure for Flexible and Smart Devices. *ACS Appl. Mater. Interfaces* **2018**, 10, 27215-27223.

(7) Zhou, P.; Chen, L.; Yao, L.; Weng, M.; Zhang, W. Humidity- and Light-driven Actuators Based on Carbon Nanotube-Coated Paper and Polymer Composite. *Nanoscale* **2018**, 10, 8422-8427.

(8) Chen, L.; Weng, M.; Zhou, P.; Zhang, L.; Huang, Z.; Zhang, W. Multi-Responsive Actuators Based on a Graphene Oxide Composite: Intelligent Robot and Bioinspired Applications. *Nanoscale* **2017**, 9, 9825-9833.

(9) Li, L.; Meng, J.; Hou, C.; Zhang, Q.; Li, Y.; Yu, H.; Wang, H. Dual-Mechanism and Multimotion Soft Actuators Based on Commercial Plastic Film. *ACS Appl. Mater. Interfaces* **2018**, 10, 15122-15128.

(10) Tang, R.; Sang, W.; Wu, Y.; Zhu, C.; Liu, J. Multi-Wavelength Light Drivable Oscillatory Actuator on Graphene-Based Bilayer Film. *Macromol. Mater. Eng.* **2017**, 302, 1600384-1600389.

(11) Tang, R.; Liu, Z.; Xu, D.; Liu, J.; Yu, L.; Yu, H. Optical Pendulum Generator Based on Photomechanical Liquid Crystalline Actuators. *ACS Appl. Mater. Interfaces* **2015**, 7, 8393-8397.

(12) Ryabchun, A.; Bobrovsky, A.; Stumpe, J.; Shibaev, V. Novel Generation of Liquid Crystalline Photo-Actuators Based on Stretched Porous Polyethylene Films. *Macromol. Rapid Commun.* **2012**, 33, 991-997.

(13) Liu, Z.; Tang, R.; Xu, D.; Liu, J.; Yu, H. Precise Actuation of Bilayer Photomechanical Films Coated with Molecular Azobenzene Chromophores. *Macromol. Rapid Commun.* **2015**, 36, 1171-1176.

(14) Li, J.; Zhang, R.; Mou, L.; Andrade, M. J.; Hu, X.; Yu, K.; Sun, J.; Jia, T.; Dou, Y.; Chen, H.; Fang, S.; Qian, D.; Liu, Z. Photothermal Bimorph Actuators with In-Built Cooler for Light Mills, Frequency Switches, and Soft Robots. *Adv. Funct. Mater.* **2019**, 29, 1808995-1809005.

(15) Wang, S.; Gao, Y.; Wei, A.; Xiao, P.; Liang, Y.; Lu, W.; Chen, C.; Zhang, C.; Yang, G.; Yao, H.; Chen, T. Asymmetric Elastoplasticity of Stacked Graphene Assembly Actualizes Programmable Untethered Soft Robotics. *Nat. Commun.* **2020**, 11, 4359-4370.

(16) Cai, G.; Ciou, J.; Liu, Y.; Jiang, Y.; Lee, P. S. Leaf-Inspired Multiresponsive MXene-Based Actuator for Programmable Smart Devices. *Sci. Adv.* **2019**, 5, eaaw7956.

Movie S1 Large bending deformation of the I-MXene film

Movie S2 Light-driven actuation of freestanding I-MXene film

Movie S3 Infrared video for the photoactuation of I-MXene film

Movie S4 Photoactuation of the bimorph actuator

Movie S5 Infrared video for the photoactuation of the bimorph actuator

Movie S6 Natural sunlight-driven actuation of the bimorph actuator

Movie S7 Continuous directional locomotion driven by natural sunlight fluctuation (4×speed)

Movie S8 Directional crawling motion driven by natural sunlight (2×speed)

Movie S9 Transportation by the robot driven by natural sunlight (2×speed)

Movie S10 Crawling motion of “inchworm” in the wild (2×speed)

Movie S11 Weight lifting of the soft arms

Movie S12 Directional crawling motion driven by the laser (4×speed)

Movie S13 Turning crawling motion driven by the laser (10×speed)